Computer Methods in Biomechanics and Biomedical Engineering, 2002 VOL. 5 (6), pp. 387–396

Taylor & Francis
Taylor & Francis Group

Virtual Power Based Algorithm for Decoupling Large Motions from Infinitesimal Strains: Application to Shoulder Joint Biomechanics

P. BÜCHLER[a,b], L. RAKOTOMANANA[c,*] and A. FARRON[b]

[a]*Institute for Biomedical Engineering, Lausanne, Switzerland;* [b]*Orthopaedic Hospital, Lausanne, Switzerland;* [c]*UFR Mathèmatiques, IRMAR—Universitè de Rennes 1, Campus Beaulieu, 35 042, Rennes Cedex, France*

(Received 20 June 2001; Revised 17 June 2002)

New trends of numerical models of human joints require more and more computation of both large amplitude joint motions and fine bone stress distribution. Together, these problems are difficult to solve and very CPU time consuming. The goal of this study is to develop a new method to diminish the calculation time for this kind of problems which include calculation of large amplitude motions and infinitesimal strains. Based on the Principle of Virtual Power, the present method decouples the problem into two parts. First, rigid body motion is calculated. The bone micro-deformations are then calculated in a second part by using the results of rigid body motions as boundary conditions. A finite element model of the shoulder was used to test this decoupling technique. The model was designed to determine the influence of humeral head shape on stress distribution in the scapula for different physiological motions of the joint. Two versions of the model were developed: a first version completely deformable and a second version based on the developed decoupling method. It was shown that biomechanical variables, as mean pressure and von Mises stress, calculated with the two versions were sensibly the same. On the other hand, CPU time needed for calculating with the new decoupled technique was more than 6 times less than with the completely deformable model.

Keywords: Virtual power based algorithm; Infinitesimal strains; Shoulder joint biomechanics; CPU time

INTRODUCTION

The long-term behavior of orthopedic prostheses depends on the bone stress distribution around the implants. The numerical approach is a sound method to determine bone stresses. Numerous numerical models have been proposed in the past for analyzing human joints as hip [1–5], knee [6,7], shoulder [8–16] or spine [17]. Most of these numerical models focus on the anchorage of the prosthesis into the bone and the boundary applied forces are predetermined by extra calculus or by experimental investigations adapted to the case in study. They do not consider the feed-back reaction of the shape of the implant to the applied joint forces. This approximation is suitable for the human joints in which the relative motion is mostly restricted by the bone structures. This is the case for joints like the hip, but this is no more the case for the shoulder glenohumeral joint, which is designed for mobility. The glenohumeral joint is composed of two bones: the humerus and the scapula. The contact surface on the humerus is spherical, while the contact surface on the scapula, which occurs in the glenoid fossa, is shallow. This particular geometry leads to a small contact area and to a large mobility. The stability of the joint is not ensured by bone structure or by ligaments but by the muscles for the major part.

In the shoulder, the stress distribution in the scapula around the glenoid component depends on the shape of the humeral component. If the shape of the humeral component changes, the glenoid bone stress distribution also changes. In order to model this effect, a new generation of numerical model should be developed. Accordingly, the models should be able to calculate both the motion of the joint and the bone stress distribution. These models should include the principal contact between the two parts of the joint and the muscles that ensure the joint stability.

To develop this model, the finite element method (FEM) remains the best approach, being the only one that can simultaneously calculate the rigid body motion

*Corresponding author. Tel.: +33-2-23-23-59-18. Fax: +33-2-23-23-67-90. E-mail: lalao@maths.univ-rennes1.fr

ISSN 1025-5842 print/ISSN 1476-8259 online
DOI: 10.1080/1025584021000016843

and the bone stress distribution. The FE method clearly allows to calculate the bone stress distribution taking the complex bone geometry into account. To evaluate the rigid body motion, other techniques have been used. For the shoulder, van der Helm [15,16] has developed a model based on inverse dynamic analysis. This model consists of rigid bones and of the line of action of every muscles of the shoulder. A kinematic analysis performed on healthy subjects was then used to calculate the force in the muscles. This method is very powerful to determine the forces in the muscle and has been used to study the influence of simple modifications of the design of the humeral prosthesis on the function of the muscles [9]. But such a model fails to determine the influence of the humeral head design on the glenohumeral motion and contact regions. First, because the kinematics is pre-determined and then because the glenohumeral contact is modeled as a perfect ball and socket joint.

Solving the problem of deformable solids undergoing large amplitude motions combined with infinitesimal strains remains difficult and CPU time consuming, essentially due to the geometrical non-linearity provoked by joint large rotations. The method is assessed by shoulder joint simulations.

To solve the problem, the idea presented here is to decouple the problem into two parts: first to calculate the rigid body motion and then the micro-deformations of the bones with the results of the first simulation as boundary conditions. The goal of the present study is to show that results obtained with a complete model and with a decoupled model are the same. And then to show that the computational resources needed to perform the simulation with the second method are smaller than for the complete model. The comparison was done with the simulation of an internal rotation of an intact shoulder.

BASIC THEORY: WEAK FORMULATION OF THE MOMENTUM BALANCE

For this purpose, we start with the Virtual Power Principle, from which equations of finite element codes are usually derived:

$$\int_{\partial\Omega} \bar{p}_n \, \mathrm{d}A \cdot w + \int_{\Omega} \rho(b - a)\mathrm{d}\Omega \cdot w = 0 \quad \forall w \tag{1}$$

where, $\bar{p}_n$, b and a are the applied contact forces on the boundary $\partial\Omega$, the body force and the absolute acceleration fields. w is an admissible virtual velocity field. The velocity v is decomposed into a rigid body velocity and into a "straining velocity" $\tilde{v}$, which may be interpreted as a superimposed motion on the rigid body motion. This later field captures the relative velocity with respect to the configuration following a rigid motion of B. Calculus of time derivative of the velocity v provides the various contributions in the absolute acceleration a:

$$v = v_G + \Omega \wedge GM + \tilde{v}$$

$$a = a_G + \dot{\Omega} \wedge GM + \Omega \wedge (\Omega \wedge GM) + \dot{\tilde{v}}_B + 2\Omega \wedge \tilde{v} \tag{2}$$

where v_G and a_G are the velocity and the acceleration of the center of mass G, respectively. Ω is the instantaneous rigid angular velocity. Notice that G is the position of center of mass after a rigid body motion. The quantity $\dot{\tilde{v}}_B$ may be interpreted as the relative acceleration of the deformable solid with respect to the rotated rigid configuration body B, we call it straining acceleration. According to Eq. (2), we can also assume a decomposition of the virtual velocity into a rigid velocity and into a straining velocity $\tilde{w}$:

$$w = w_G + \Omega_w \wedge GM + \tilde{w} \tag{3}$$

where w_G is a virtual velocity of G, and Ω_w a virtual angular velocity of the solid. In the following, we show that the present method includes the rigid body dynamics description and the classical continuum mechanics description.

Rigid Body Dynamics ($\tilde{v} = 0$ And $\tilde{w} = 0$)

Consider a rigid body velocity, acceleration and virtual velocity as follows:

$$v = v_G + \Omega \wedge GM \quad w = w_G + \Omega_w \wedge GM$$

$$a = a_G + \dot{\Omega} \wedge GM + \Omega \wedge (\Omega \wedge GM) \tag{4}$$

By introducing Eq. (4) in Virtual Power Principle [Eq. (1)], we obtain the following relation for $\forall w_G$, $\forall \Omega_w$:

$$\int_{\partial\Omega} \bar{p}_n \, \mathrm{d}A \cdot w_G + \int_{\Omega} \rho(b - a_G)\mathrm{d}\Omega \cdot w_G$$

$$+ \int_{\Omega} \rho(-\dot{\Omega} \wedge GM - \Omega \wedge (\Omega \wedge GM))\mathrm{d}\Omega \cdot w_G$$

$$\int_{\partial\Omega} (GM \wedge \bar{p}_n)\mathrm{d}A \cdot \Omega_w + \int_{\Omega} \rho(GM \wedge b - a_G))\mathrm{d}\Omega \cdot \Omega_w$$

$$- \int_{\Omega} \rho[\dot{\Omega} \wedge GM + \Omega \wedge (\Omega \wedge GM)]\mathrm{d}\Omega \cdot (\Omega_w \wedge GM)$$

$$- \int_{\Omega} \sigma : \nabla(w_G + \Omega_w \wedge GM)\mathrm{d}\Omega = 0 \tag{5}$$

Relation equation (5) may be simplified by introducing the inertial tensor of the solid I_G calculated at the center of mass G, which is the position of the body mass center after rigid motion:

$$\int_{\Omega} \rho(\dot{\Omega} \wedge GM) \cdot (\Omega_w \wedge GM)\mathrm{d}\Omega = (I_G \dot{\Omega}) \cdot \Omega_w \tag{6}$$

$$\int_\Omega \rho[\Omega\wedge(\Omega\wedge GM)]\mathrm{d}\Omega\cdot(\Omega_w\wedge GM)=(\Omega\wedge I_G\Omega)\cdot\Omega_w \quad (7)$$

with the inertial tensor $I_G=\int_\Omega\rho[\|GM\|^2-(GM\otimes GM)]\mathrm{d}\Omega$. By defining the virtual spin tensor $\bar{\Omega}_w$ as $\Omega_w\wedge OM=\bar{\Omega}_w(OM)$, we find:

$$\int_\Omega\sigma:\nabla(w_G+\Omega_w\wedge GM)\mathrm{d}\Omega=\int_\Omega\sigma:\nabla[\Omega_w\wedge(OM-OG)]\mathrm{d}\Omega$$

$$=\int_\Omega\frac{1}{2}(\sigma-\sigma^T):\bar{\Omega}_w\mathrm{d}\Omega=0 \quad (8)$$

due to the symmetry of stress tensor σ. Then, the following holds $\forall w_G$ for and $\forall\Omega_w$:

$$\left[\int_{\partial\Omega^p}\bar{p}_n\mathrm{d}A+\int_\Omega\rho b\mathrm{d}\Omega\right]\cdot w_G$$

$$+\left[\int_{\partial\Omega^p}GM\wedge\bar{p}_n\mathrm{d}A+\int_\Omega\rho GM\wedge b\mathrm{d}\Omega\right]\cdot\Omega_w$$

$$=m\dot{v}_G\cdot w_G+[I_G\dot{\Omega}+\Omega\wedge I_G\Omega]\cdot\Omega_w \quad (9)$$

By choosing specific virtual velocity fields, we deduce the system of equations governing the rigid body dynamics respectively for linear momentum $\forall w_G\neq 0$, $\Omega_w=0$ and for angular momentum $w_G=0$, $\forall\Omega_w\neq 0$:

$$\begin{cases}\int_{\partial\Omega^p}\bar{p}_n\,\mathrm{d}A+\int_\Omega\rho b\,\mathrm{d}\Omega=m\dot{v}_G\\ \int_{\partial\Omega^p}GM\wedge\bar{p}_n\,\mathrm{d}A+\int_\Omega\rho GM\wedge b\,\mathrm{d}\Omega\\ \quad=I_G\dot{\Omega}+\Omega\wedge I_G\Omega\end{cases} \quad (10)$$

Dynamics of Deformable Solids

By analogy, the introduction of the real velocity and acceleration fields and the virtual velocity field Eqs. (2) and (3) in Eq. (1) allows to obtain the complete weak form of the Principle of Virtual Power:

$$\int_{\partial\Omega^p}\bar{p}_n\,\mathrm{d}A\cdot w_G+\int_\Omega\rho(b-a_G)\mathrm{d}\Omega\cdot w_G-\int_\Omega\rho\dot{\bar{v}}_B\,\mathrm{d}\Omega\cdot w_G$$

$$+2\Omega\wedge\int_\Omega\rho\tilde{v}\mathrm{d}\Omega\cdot w_G+\int_{\partial\Omega^p}GM\wedge\bar{p}_n\,\mathrm{d}A\cdot\Omega_w$$

$$+\int_\Omega[GM\wedge\rho b-GM\wedge\rho\dot{\bar{v}}_B-2GM\wedge\rho(\Omega\wedge\tilde{v})]\cdot\Omega_w\,\mathrm{d}\Omega$$

$$-(I_G\dot{\Omega}+\Omega\wedge I_G\Omega)\cdot\Omega_w+\int_{\partial\Omega^p}\bar{p}_n\,\mathrm{d}A\cdot\tilde{w}$$

$$+\int_\Omega\rho[b-a_G-\dot{\Omega}\wedge GM-\Omega\wedge(\Omega\wedge GM)-\dot{\bar{v}}_B$$

$$-2\Omega\wedge\tilde{v}]\mathrm{d}\Omega\cdot\tilde{w}-\int_\Omega\sigma:\nabla\tilde{w}\,\mathrm{d}\Omega=0$$

This equation includes three coupled equations.

1. For virtual translation velocity $w_G\neq 0$, $\Omega_w=0$, and $\tilde{w}=0$, it reads:

$$\int_{\partial\Omega^p}\bar{p}_n\,\mathrm{d}A\cdot w_G+\int_\Omega\rho b\,\mathrm{d}\Omega\cdot w_G-\int_\Omega\rho\dot{\bar{v}}_B\,\mathrm{d}\Omega\cdot w_G$$

$$+2\Omega\wedge\int_\Omega\rho\tilde{v}\,\mathrm{d}\Omega\cdot w_G=m\dot{v}_G\cdot w_G \quad (11)$$

where the two last terms of the left-hand-side may be interpreted as the coupling effects of the inertial forces and Coriolis forces due to straining motion.

2. For virtual rotations $w_G=0$, $\Omega_w\neq 0$, and $\tilde{w}=0$, we have:

$$\int_{\partial\Omega^p}GM\wedge\bar{p}_n\,\mathrm{d}A\cdot\Omega_w+\int_\Omega[GM\wedge(\rho b-\rho\dot{\bar{v}}_B$$

$$-2\rho\Omega\wedge\tilde{v})]\cdot\Omega_w\,\mathrm{d}\Omega=[I_G\dot{\Omega}+\Omega\wedge(I_G\Omega)]\cdot\Omega_w \quad (12)$$

3. Finally, for straining virtual velocity, $w_G=0$, $\Omega_w=0$, and $\tilde{w}\neq 0$, the deformation of the solid is described by:

$$\int_{\partial\Omega^p}\bar{p}_n\,\mathrm{d}A\cdot\tilde{w}+\int_\Omega\rho[b-a_G-\dot{\Omega}\wedge GM$$

$$-\Omega\wedge(\Omega\wedge GM)]\mathrm{d}\Omega\cdot\tilde{w}$$

$$-\int_\Omega\rho(\dot{\bar{v}}_B+2\Omega\wedge\tilde{v})\mathrm{d}\Omega\cdot\tilde{w}=\int_\Omega\sigma:\nabla\tilde{w}\,\mathrm{d}\Omega \quad (13)$$

In these three equations, the unknown variables are v_G, Ω and $\tilde{v}$. The system of governing coupled equations writes in weak form:

$$\begin{cases}\int_{\partial\Omega^p}\bar{p}_n\,\mathrm{d}A\cdot w_G+\int_\Omega\rho b\,\mathrm{d}\Omega\cdot w_G-\int_\Omega\rho\dot{\bar{v}}_B\,\mathrm{d}\Omega\cdot w_G\\ \quad+2\Omega\wedge\int_\Omega\rho\tilde{v}\,\mathrm{d}\Omega\cdot w_G=m\dot{v}_G\cdot w_G\\ \int_{\partial\Omega^p}GM\wedge\bar{p}_n\,\mathrm{d}A\cdot\Omega_w+\int_\Omega[GM\wedge(\rho b-\rho\dot{\bar{v}}_B\\ \quad-2\rho\Omega\wedge\tilde{v})]\cdot\Omega_w\,\mathrm{d}\Omega=[I_G\dot{\Omega}+\Omega\wedge(I_G\Omega)]\cdot\Omega_w\\ \int_{\partial\Omega^p}\bar{p}_n\,\mathrm{d}A\cdot\tilde{w}+\int_\Omega\rho[b-a_G-\dot{\Omega}\wedge GM\\ \quad-\Omega\wedge(\Omega\wedge GM)]\mathrm{d}\Omega\cdot\tilde{w}-\int_\Omega\rho(\dot{\bar{v}}_B+2\Omega\wedge\tilde{v})\mathrm{d}\Omega\cdot\tilde{w}\\ \quad=\int_\Omega\sigma:\nabla\tilde{w}\,\mathrm{d}\Omega\end{cases} \quad (14)$$

For decoupling the straining velocity ($\tilde{v}$) from rigid body motions (v_G and Ω) we propose the following:

1. *Step 1*: Calculate an approximate value $\hat{v}_G$ of v_G and approximate rotation velocity $\hat{\Omega}$ of Ω with rigid body dynamics equations (10). This means to neglect the influence of $\tilde{v}$ in Eqs. (11) and (12).
2. *Step 2*: Calculate the new configuration of the body due to this rigid displacement $\hat{OG}$ and $\hat{GM}$.

3. *Step 3*: Introduce the pre-defined values $\dot{v}_G$, $\hat{\Omega}$, $\dot{OG}$ and $\dot{GM}$ in Eq. (13) and then solve to obtain $\tilde{v}$ to have the deformed configuration of the deformable solid where $\dot{\tilde{v}}_B$ may be estimated with the Jaumann derivative (e.g. Rakotomanana, 1998) $\dot{\tilde{v}}_B \approx \tilde{v}_{\tilde{v}} - \hat{\Omega} \wedge \tilde{v}$.

The following overall algorithm holds:

$$\left\{ \begin{array}{l} \left. \begin{array}{l} \int_{\partial\Omega^p} \bar{p}_n \, dA + \int_\Omega \rho b \, d\Omega = m\dot{v}_G \\ \int_\Omega GM \wedge \rho b \, d\Omega \\ \quad + \int_{\partial\Omega^p} GM \wedge \bar{p}_n \, dA \\ \quad = I_G \dot{\Omega} + \Omega \wedge (I_G \Omega) \end{array} \right\} \Rightarrow (\hat{v}_G, \hat{\Omega}) \Rightarrow (\hat{OG}, \hat{GM}) \\ \int_{\partial\Omega^p} \bar{p}_n \, dA \cdot \tilde{w} + \int_\Omega \rho [b - \hat{a}_G - \hat{\Omega} \wedge \hat{GM} \\ \quad - \hat{\Omega} \wedge (\hat{\Omega} \wedge \hat{GM})] d\Omega \cdot \tilde{w} \\ \quad - \int_\Omega \rho (\dot{\tilde{v}}_B + 2\hat{\Omega} \wedge \tilde{v}) d\Omega \cdot \tilde{w} = \int_\Omega \sigma : \nabla \tilde{w} \, d\Omega \end{array} \right.$$

EXPERIMENTAL

A finite element model of an intact human shoulder was reconstructed. Two numerical algorithms were developed. Both of the two algorithms were applied to solve one problem with the same boundary conditions based on the same geometric reconstruction of the shoulder. The first algorithm considers simultaneously the rigid body motion and the bone stress with deformable bones. The second algorithm is a two-steps simulation. In the first step bones are assumed to be rigid and only the rigid body motion of the joint is calculated. The bone stress is calculated in the second step of the simulation. Simulations of the same load case, which corresponds to an internal rotation of the shoulder from 0 to 60°, were performed with the two different approaches.

Description of the 1 Step Method (Method #1)

The model development includes the following steps: (1) the data acquisition, (2) the reconstruction of the model and (3) the simulation of various biomechanical and clinical situations. A normal (without any evidence of pathology) fresh frozen cadaveric shoulders was used.

Data Acquisition

Bone: A CT scan of the shoulder was performed (helicoidal CT, General Electric). Slices (1 mm thick) were obtained from the acromion to the middle portion of the humerus. CT provided data about bone geometry, and bone density distribution.

Soft tissues: The three major rotator cuff muscles and tendons were included in the model: subscapularis, supra and infraspinatus. A careful dissection of both shoulders was performed for this purpose. The insertions of the three muscles on the humerus and the scapula were accurately located. Using a Polhemus 3 space Fastrak Stylus and the 3-axis coordinate system application [18], we digitized the exact insertion and origin of the three muscles. Four points at the corner of each muscle (8 points per muscle) were recorded to represent the insertions.

Landmarks: For the model reconstruction, it is mandatory to have all data (soft tissues, bone and cartilage) in the same coordinate system. To this end, 12 zirconium beads, 0.5 mm of diameter, were implemented percutaneously, before the CT scan, in the bone cortex of each shoulder (6 in the humerus and 6 in the scapula). Their positions were then accurately located during dissection and digitized using the Polhemus. As the zirconium beads were also visible on CT, it was possible to use of all data in the same coordinate system.

Model Reconstruction

3D-bone geometry: The external contour of bone was accurately defined on each CT slice with a digitization error lower than 0.7 mm (2 pixels). The obtained curves were then transferred in the PATRAN software (MacNeal-Schwendler, GmBH) and the three-dimensional geometry of the scapula and of the proximal humerus of the shoulder was reconstructed. The three-dimensional finite element meshes of the bones (scapula and humerus) were thus generated using hexahedral elements from the reconstructed geometry (Fig. 1). To mesh the bones, 16541 elements were used. Both spongious and cortical bone were considered. Their mechanical properties were directly related to the bone density calculated at each node of the model from the CT-scan images. A custom-made software was designed to read the density from CT

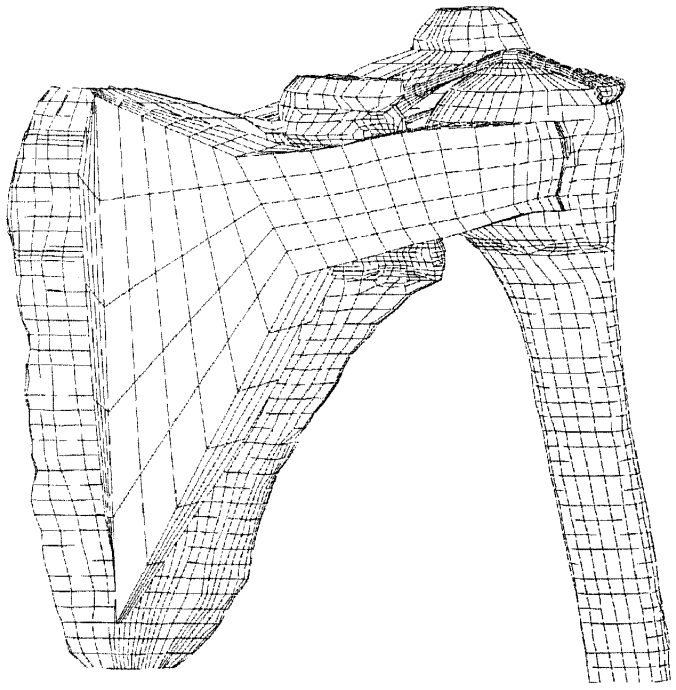

FIGURE 1 Finite element mesh of bones and muscles.

TABLE I Description of the constitutive laws used in the model

Element	Type of the law	Mathematical expression	Constants	References
Bone	Linear elastic non-homogenous	$E = E_0\left(\frac{\rho}{\rho_0}\right)^2$, $\nu = \nu_0$	$E_0 = 15,000$ [MPa], $\nu_0 = 0.3$, $\rho_0 = 1.8$ [g/cm^3], ρ : bone density	[24–26]
Muscles	Exponential hyperelastic incompressible	$W = \alpha \exp[\beta(I_1 - 3)] - \frac{\alpha\beta}{2}(I_2 - 3)$	$\alpha = 0.12$ [MPa], $\beta = 1.0$	[21–23]
Cartilage	Neo-Hookean hyperelastic incompressible	$W = C_{10}(I_1 - 3)$ where $C_{10} = \frac{E}{4(1+\nu)}$	$C_{10} = 1.79$ ($E = 10$ [MPa], $\nu = 0.4$)	[27]

I_1 and I_2 are the first and second invariants of the Cauchy-Green tensor.

slices and to incorporate automatically the non-homogeneous distribution of bone density into the meshes. This software first read all the CT images, compute a relative density for each node of the mesh and then save the resulting list in an output file [5]. The mechanical properties of bone depend on the square of the apparent density (Table I). According to this quadratic dependency, a non-homogeneous bone constitutive law was developed [19,20] and implemented in the ABAQUS software (Hibbitt, Karlsson and Sorensen, Inc.).

Soft tissues: The geometry of the subscapularis, supra and infraspinatus muscles was 3D reconstructed. We considered the muscular origins and insertions on the bone surface as defined by the four digitized landmarks on the scapula and humerus, respectively. The muscular belly was assumed to be the isoparametric solid between the two insertion surfaces, accounting for the previously reconstructed bone geometry. Three-dimensional muscles were then meshed with about 800 hexahedral elements (Fig. 1). Muscles were assumed to be incompressible and hyperelastic allowing large strains. In the present study, only the passive behavior of the muscles was accounted for. Muscles passive stress–strain law (Table I) was based on the strain energy function of Veronda [21] and has been recently applied for other joint soft tissue as ligaments and tendons [22,23].

Cartilage: The articular cartilage of the shoulder was also reconstructed. The reconstruction was based on the hypothesis that the space observed on the CT images between the humerus and scapula is filled with cartilage. The minimum gap was measured and the cartilage was 3D reconstructed with a constant thickness equal to the half of this distance. The finite element mesh was made of 2868 hexahedral elements. A Neo-Hookean incompressible constitutive law was used for cartilage (Table I).

Interfaces: We used a discontinuous unilateral large sliding interface between the scapula and the humerus. This contact law allowed calculating the normal stress and shear stress at the glenohumeral interface. A discontinuous unilateral small sliding interface was assumed between the three reconstructed muscles and the bones. Muscles are allowed to slide on the bone surfaces except at the muscular insertion zones.

Boundary conditions: The scapula was not rigidly fixed but was maintained by 20 flexible elements replacing the stabilizing muscles of the scapula: the trapezius, the rhomboideus major and the rhomboideus minor. The gliding of the scapula on the thorax was also reconstructed by introducing a flexible element in the antero-posterior direction. The distal section of the humerus was fixed by four vertical flexible elements, precluding any significant movement in abduction.

Simulations

The neutral position of the glenohumeral joint was defined as the position when the center of the humeral articular surface faces the center of the glenoid fossa. From this neutral position an internal rotation up to 60° was simulated. The rotation was achieved by imposing displacement of the scapular insertion of the subscapularis muscle whereas the supraspinatus and infraspinatus muscles were inserted at both ends of the bones. This induced a gradual and controlled rotation of the humerus. ABAQUS/Standard 5.8 is used for the simulations. The computer on which the calculations were performed is a Dec/alpha.

Description of the 2 Steps Method (Method #2)

The second method is based on the same reconstruction than the first method. This methods consists in two simulations: first a simulation to calculate the rigid body motion and then the second to determine the bone stress distribution.

Part 1—Rigid Body Motion

In this part, the bones are considered as rigid. The only difference with the first model is the bone mesh. Since the bones are rigid, the hexahedral mesh of the bone volume is replaced by a mesh of the external surface of the bones with 2795 quadrilateral first order elements (humerus: 929, scapula and spinatus: 1866).

The boundary conditions on the humerus and scapula are the same as before. The only difference is that the contacts between the bones and muscles are rigid/deformable instead of deformable/deformable contacts. The glenohumeral contact is not changed, it still occurs between the humeral and scapular cartilage. But this time, the cartilage is not fixed on the underling bones but on the corresponding rigid surface. The simulation is the same as with the first method. It also corresponds to an internal rotation of 60°. The rotation is obtained by the same displacement of the subscapularis muscle.

The results obtained with this simulation are the relative glenohumeral motion, the contact pressure on the glenoid fossa and the muscular forces. Some of these results are needed for the second part of the simulation. The forces on each node of the glenoid fossa and the displacements of nodes located in the middle part of the muscles. The force on each node of the glenoid is obtained with the ABAQUS output variable NFORC. This variable gives for each node of an element the forces due to the stresses in the element. The sum of all these contributions for a node in contact, gives the force due to the contact acting at that node. A C++ software was created to automatically read the ABAQUS output files, compute the force on each node of the glenohumeral contact and write a file containing the loads for the second part of the simulation. Similarly, a second C++ software was developed to write a file containing the displacement of the nodes selected in the middle part of the muscles.

Part 2—Bone Stress Determination

In this part, the mesh of the scapula is the same as with the first method, but this time the humerus is no more included in the model. The humerus is replaced by its effect: the forces on the glenohumeral contact replace the contact itself and the displacements of the muscles replace the displacements of the humerus.

The boundary conditions on the scapula are defined by the first part of the simulation. The contact forces and nodal displacements calculated in the first part are imposed on the scapula. Furthermore, the scapula is still maintained by flexible elements. This calculation gives the bone micro-deformations and thus the bone stress distribution.

RESULTS

Contact Pressure

The contact pressure on the glenoid fossa during internal rotation from 0 to 60° is represented in Fig. 2. The contact region on the glenoid was the same with the two methods. The value of the maximum contact pressure is lower with the second method at 30 and 40° rotation but higher at 50 and 60° rotation. The maximum error on the contact pressure calculated with the two methods is less than 5% at 40° internal rotation.

Forces in the Muscles

Figure 3 represents the force in two muscles of the rotator cuff. The forces were calculated during the rotation. The force calculated with the rigid approximation is always smaller than the force calculated with the deformable method. The error increases during the rotation. The maximum error is for the infraspinatus muscle at 60° rotation and is less than 1%.

Von Mises Stress—distribution in a slice

The von Mises stress in the scapula was calculated with the two methods. The stress distribution obtained with both methods is represented in Fig. 4 in a horizontal cut of the scapula. The level of the cut was chosen at the same level than the glenohumeral contact. At this level, the distribution of von Mises stress is the same with the two methods. Only the maximal values differ. At this level the maximal stress calculated with the first method is about 5% higher.

Von Mises Stress—in the Whole Scapula

The von Mises stress was calculated in the whole scapula. The results were then extrapolated to the nodes. Figure 5a a represents the von Mises stress obtained with the two methods. Each point of the graphic represents one node. The x-value is the stress obtained with the first method and the y-value is the stress with the second method. In the case of two exactly equivalent methods, all the points should lie on a straight line with the equation $y = x$. In the present case there is a linear correlation between the two methods with a correlation coefficient of 0.999.

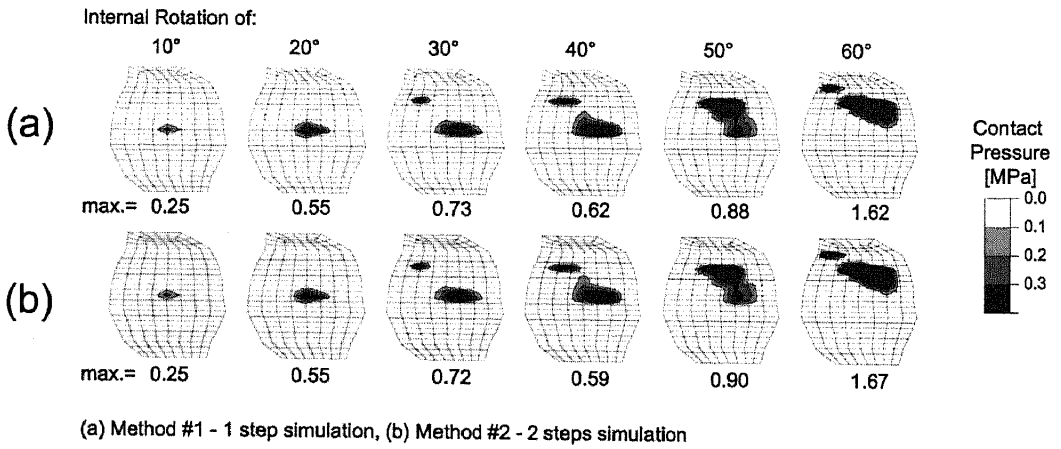

FIGURE 2 Comparison of the calculated contact pressure on the glenoid fossa during a progressive internal rotation from 0 to 60°.

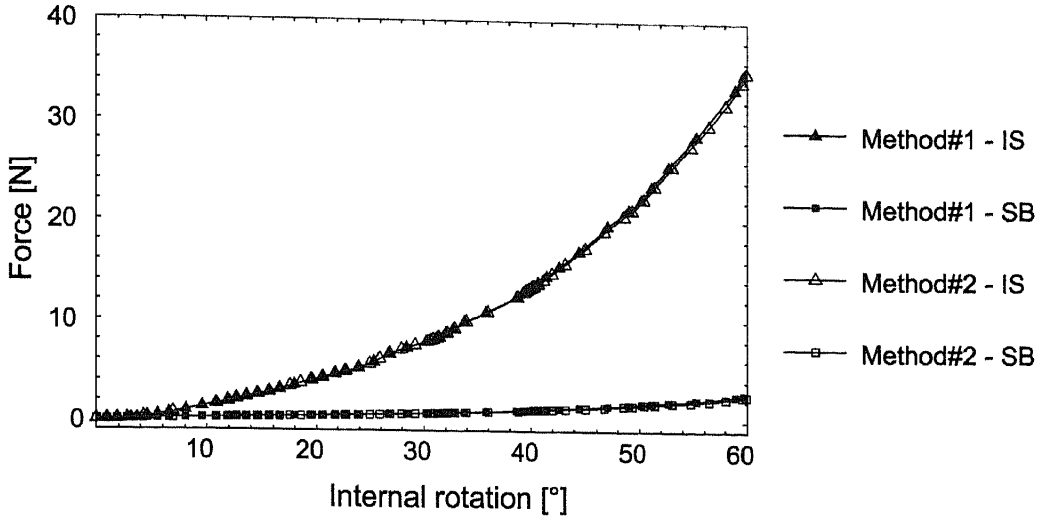

FIGURE 3 Force in the InfraSpinatus (IS) and SubScapularis (SB) muscle during the rotation calculated with the two methods.

But the equation of the line obtained with the least mean square methods is: $y = 0.98x$. This indicates that the stresses calculated with the first method are smaller than the stress calculated with the second method. The figure shows also that this bias is more important for the higher values of the stress.

The distribution of the error between the methods is reported in Fig. 5b. The distribution has the majority of the points around 0. We can conclude that the two methods give the same results. Again, a small bias can be observed: the mean of the distribution is at 0.012 indicating that the values obtained with the first method are higher than with the second method. Furthermore, the figure clearly indicates that the distribution is unbalanced on the right, indicating that there are more points for which the stress calculated with the first method is higher.

Computer Resources Needed for the Simulations

The resources needed to run the different simulations are reported in Table II. The most important parameter is the time needed for the simulation. With the second method the CPU time is more than 6 times less than with the first method (22h30 vs. 3h40). Other parameters are also important to determine the size of the simulations: like the memory needed (70% decrease with the second method) or the total disk space needed for the simulation (43% decrease with the second method).

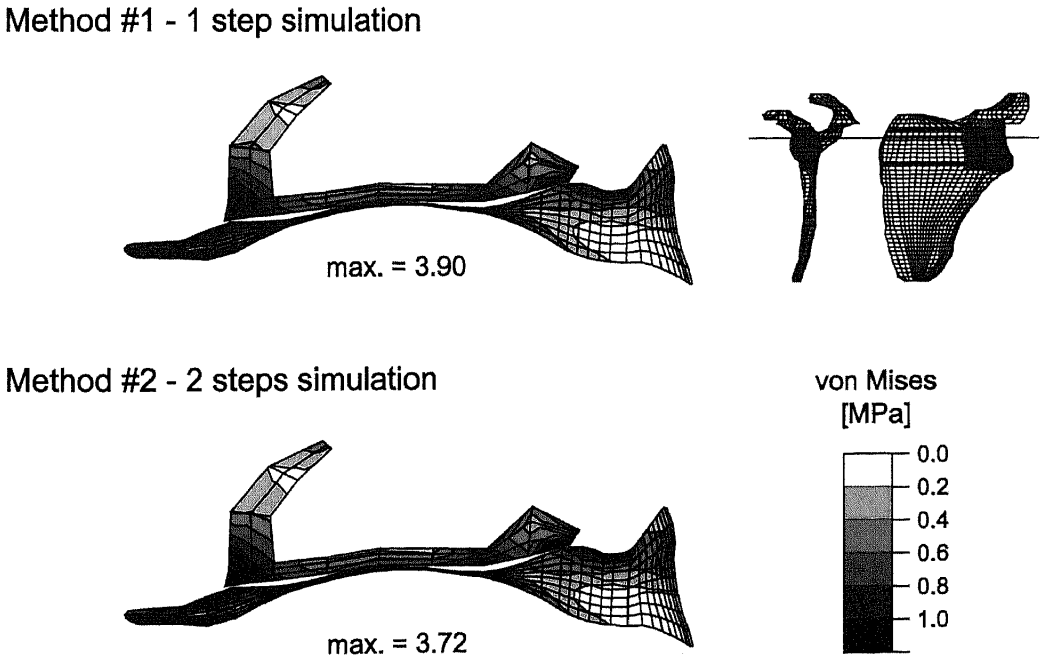

FIGURE 4 Von Mises stresses distribution at 60° internal rotation in an horizontal cut of the scapula with the two methods. The cut is performed at the level of the glenohumeral contact.

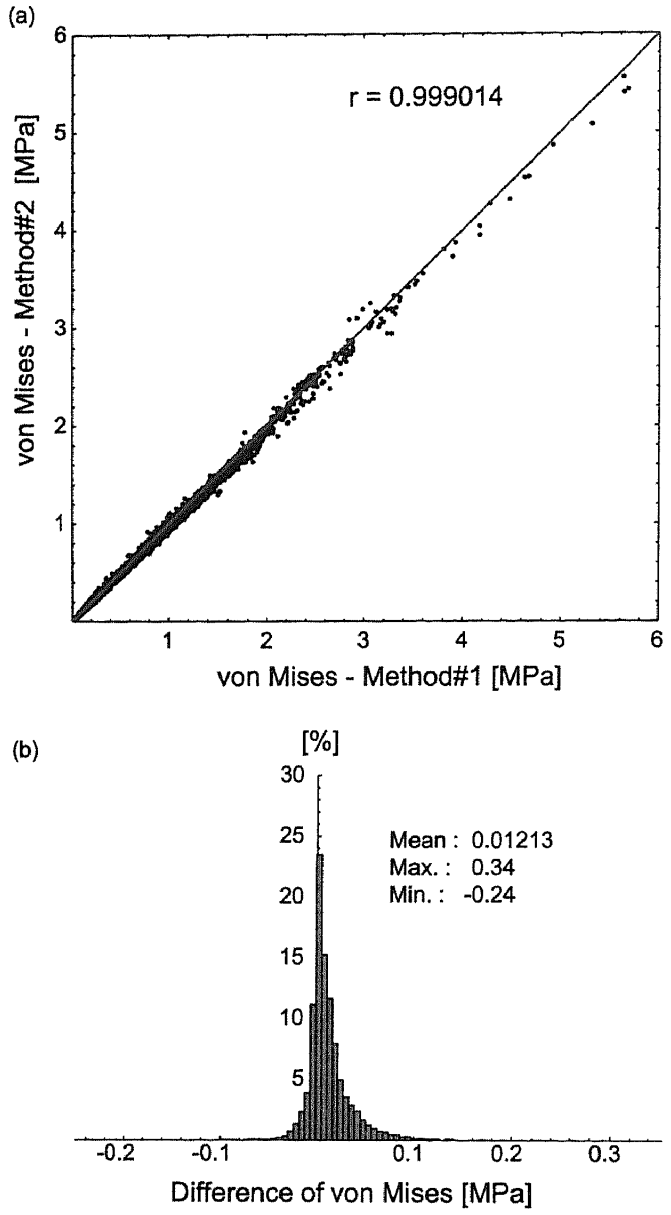

FIGURE 5 The von Mises stresses calculated for each node of the scapula with the two methods are plotted in graph (a). The correlation coefficient is 0.999 showing a clear linear correlation between the two methods. The gray curve indicates the ideal position for the points (i.e. $y = x$). Graph (b) shows the percentage of node with a given error.

DISCUSSION

The main interest of the developed method is the computer time saving. The method consists in solving first a discrete variational problem with six degrees of freedom (Eqs. (10) and (13)) and therefore to use this approximate solution as predictor for the deformable problem, prior to the first iteration on displacement. The more this predictor is close to the solution of the deformable problem, the more the method is efficient and the convergence enhanced. This is expectably the case whenever the terms in $\tilde{v}$ and its time derivatives in Eqs. (11) and (12) are sufficiently small with respect to the other variables. The application of this theory in shoulder biomechanics is validated. An internal rotation of an intact joint was simulated with the two methods: first without decoupling and then with the decoupling methods. Qualitatively, the results obtained with the two methods were the same. But the time needed for the simulation using the decoupling theory was about six times lower.

Quantitatively, there are some slight differences between the two methods. The forces in the infraspinatus and subscapularis muscles are the same during the entire rotation. The error between the methods is less than 1%. For the glenohumeral contact, although the contact region is exactly the same with the two methods, there is a difference in the value of the maximal contact pressure. With the new method there is an error of less than 5% on the maximum contact pressure. But the higher value is not always computed with the same methods. This indicates that there are small differences in the glenohumeral motion, even for the same angle of rotation. These differences may be due to the fact that the deformable humerus could undergo some bending deformations which is not the case for the rigid one.

The stress distribution in the scapula calculated with the two methods is the same. The comparison of the von Mises stress for each node of the scapula indicates a strong linear correlation between the methods. However a small bias between the methods can be observed: the stress calculated with the new method is smaller than with the first method. Two observations lead to this conclusion. First, the slope of the least mean square equation is 0.98 and not 1. Second, the distribution of the difference of stress is not symmetric. There are more points for which the stress calculated with the first method is higher than with the second method. The very strong linear correlation between the methods could be used to correct the results obtained with the new method.

However, in biomechanics like in many other cases, only the general behavior of the problem is of interest. We are not often interested in the exact value of the stress or contact pressure, but rather on their parametric behavior. In this way, many other approximations in the model are more important than the few percents observed between the two methods presented here. And one of the first approximation is the FE method itself with its spatial approximation.

TABLE II Comparison of the computer resources needed for the simulations with the two methods

	CPU time [s]		Memory [MB]	Temporary disk space [MB]	Disk space [MB] (results)
Method #1	81,263		295	1536	1112
Method #2—part 1 (rigid body)	11,836	Total 13,346	86	667	190
Method #2—part 2 (bone stress)	1509		61	290	88

The great advantage of the new method is the decrease in the computer resources needed and especially the decrease of the CPU time. In the example presented here, the time needed to achieve the simulation with the second method is more than six times lower than with the first method. The need in other computer resources is also decreased. The need in memory is more than 70% lower and the disk space used for the new method is 43% the space of old method. With this new method, the same simulation runs faster on the same computer.

Since the goal of this study is to decrease the CPU time, the effect of the constitutive laws chosen in the model on the calculation time has to be examined. Assuming a homogenous constitutive law for bone does not significantly decrease the CPU time. This justifies the use of the bone non-homogeneous constitutive law. On the other side, non-homogeneity of spongious bone cannot be neglected if the model is applied to analyze the anchorage of orthopedic prostheses. The soft tissue constitutive laws have been chosen as simple as possible in this work. Hyper-elasticity is necessary for modeling large deformation of the soft tissue. We have observed that CPU time does not sensibly depend on the shape of the chosen hyper-elastic law. Exponential shape of the muscular law corresponds to the usual behavior of the soft tissue and the neo-hookean constitutive law used for the cartilage is the simplest one that holds for the large compression strain supported by this constituent.

The method presented here is interesting for the evaluation of the model sensitivity to the mechanical properties of soft tissues. The determination of constants used in the constitutive laws is difficult. This is mainly due to the limited number of data existing in the literature about mechanical properties of soft tissues, especially of the muscles. In this way, parametric studies on constants introduced in soft tissue constitutive laws will be conducted in the future to evaluate the sensitivity of the model to these mechanical properties. The decoupling method presented here will help to carry out this sensitivity analysis with a significant decrease of the CPU time.

In the particular case of the model of the shoulder presented here, the new method is even more interesting when we wanted to deal with prostheses. Two reasons for that: first the model became more complex due to the presence of the prosthesis, the cement around the prosthesis and the fine bone mesh around the cement. The number of elements and thus the number of degree of freedom become huge. For example, a model with a Neer hemiarthoplasty has been developed and has about 106,000 degrees of freedom. This number has to be compared to the 84,000 degrees of freedom of the deformable model of the intact shoulder (22h30 of simulation). The second reason is that prostheses are very rigid. Most prostheses are made in metal, often in titanium, Ti–Al–V alloy or Co–Cr alloy. So it is possible to consider the prosthetic humeral head as rigid. This approximation decreases again the size of the problem, because the deformable/deformable large sliding contact is replaced by a deformable/rigid large sliding contact.

When we have to deal with big problems of deformable solids undergoing large motions, the decoupling approach presented here constitutes a promising solution since it dramatically diminish the CPU time and all the other computer resources needed for the simulation without significant modifications of the results. This is especially useful in joint biomechanics when both the joint motion and the bone stress distribution have to be calculated. One of the most important benefit of this approach is to give the opportunity to make parametric studies. But this also gives the possibility to add more complexity on the model. For example to include more muscles in the shoulder model.

References

[1] Biegler, F.B., Reuben, J.D., Harrigan, T.P., Hou, F.J. and Akin, J.E. (1995) "Effect of porous coating and loading conditions on total hip femoral stem stability", *J. Arthroplasty.* **10**, 839–847.

[2] Huiskes, R. and van Rietbergen, B. (1995) "Preclinical testing of total hip stems. The effects of coating placement", *Clin. Orthop.*, 64–76.

[3] Ramaniraka, N.A., Rakotomanana, L.R. and Leyvraz, P.F. (2000) "The fixation of the cemented femoral component. Effects of stem stiffness, cement thickness and roughness of the cement-bone surface", *J. Bone Jt Surg. Br.* **82**, 297–303.

[4] Rubin, P.J., Rakotomanana, R.L., Leyvraz, P.F., Zysset, P.K., Curnier, A. and Heegaard, J.H. (1993) "Frictional interface micromotions and anisotropic stress distribution in a femoral total hip component", *J. Biomech.* **26**, 725–739.

[5] Terrier, A., Adaptation of Bone to Mechanical Stress: Theoretical Model, Experimental Identification and Orthopedic Applications Ph.D. Thesis (Lausanne).

[6] Farron, A., Rakotomanana, R.L., Zambelli, P.Y. and Leyvraz, P.F. (1995) "Total knee prosthesis. Clinical and numerical study of micromovements of the tibial implant", *Rev. Chir. Orthop. Reparatrice Appar. Mot.* **80**, 28–35.

[7] Rakotomanana, R.L., Leyvraz, P.F., Curnier, A., Heegaard, J.H. and Rubin, P.J. (1992) "A finite element model for evaluation of tibial prosthesis-bone interface in total knee replacement", *J. Biomech.* **25**, 1413–1424.

[8] Barèa, C., Modelisation 3D par al mèthode des èlèments finis d'une articulation scapulo-humèrale. Application á l'ètude des contraintes sur une èpaule saine avec differents types de glénes prothètiques Ph.D. Thesis University Paul Sabatier (Toulouse).

[9] de Leest, O., Rozing, P.M., Rozendaal, L.A. and van der Helm, F.C. (1996) "Influence of glenohumeral prosthesis geometry and placement on shoulder muscle forces", *Clin. Orthop.*, 222–233.

[10] Friedman, R.J., LaBerge, M., Dooley, R.L. and O'Hara, A.L. (1992) "Finite element modeling of the glenoid component: Effect of design parameters on stress distribution", *J. Shoulder Elbow Surg.* **1**, 261–270.

[11] Lacroix, D., Murphy, L.A. and Prendergast, P.J. (2000) "Three-dimensional finite element analysis of glenoid replacement prostheses: a comparison of keeled and pegged anchorage systems", *J. Biomech. Eng.* **122**, 430–436.

[12] Lacroix, D. and Prendergast, P.J. (1997) "Stress analysis of glenoid component designs for shoulder arthroplasty", *Proc. Inst. Mech. Eng. [H]* **211**, 467–474.

[13] Orr, T.E., Carter, D.R. and Schurman, D.J. (1988) "Stress analyses of glenoid component designs", *Clin. Orthop.*, 217–224.

[14] Stone, K.D., Grabowski, J.J., Cofield, R.H., Morrey, B.F. and An, K.N. (1999) "Stress analyses of glenoid components in total shoulder arthroplasty", *J. Shoulder Elbow Surg.* **8**, 151–158.

[15] van der Helm, F.C. (1994) "Analysis of the kinematic and dynamic behavior of the shoulder mechanism", *J. Biomech.* **27**, 527–550.

[16] van der Helm, F.C. (1994) "A finite element musculoskeletal model of the shoulder mechanism", *J. Biomech.* **27**, 551–569.
[17] Villarraga, M.L., Anderson, R.C., Hart, R.T. and Dinh, D.H. (1999) "Contact analysis of a posterior cervical spine plate using a three-dimensional canine finite element model", *J. Biomech. Eng.* **121**, 206–214.
[18] Karduna, A.R., Williams, G.R., Williams, J.L. and Iannotti, J.P. (1996) "Kinematics of the glenohumeral joint: influences of muscle forces, ligamentous constraints, and articular geometry", *J. Orthop. Res.* **14**, 986–993.
[19] Rakotomanana, L.R., Terrier, A., Ramaniraka, N.A. and Leyvraz, P.F. (1999) "Anchorage of orthopaedic prostheses: influence of bone properties and bone-implant mechanics", In: Pedersen, P. and Bendsøe, M., eds, Synthesis in Bio Solid Mechanics (Kluwer Academic Publishers, Dordrecht), pp. 55–66.
[20] Terrier, A., Rakotomanana, L., Ramaniraka, N. and Leyvraz, P.F. (1997) "Adaptation models of anisotropic bone", *Comput. Methods Biomech. Biomed. Eng.* **1**, 47–59.
[21] Veronda, D.R. and Westmann, R.A. (1970) "Mechanical characterization of skin-finite deformations", *J. Biomech.* **3**(1), 111–124.
[22] Pioletti, D.P., Rakotomanana, L.R., Benvenuti, J.F. and Leyvraz, P.F. (1998) "Viscoelastic constitutive law in large deformations: application to human knee ligaments and tendons", *J. Biomech.* **31**, 753–757.
[23] Pioletti, D.P., Rakotomanana, L.R. and Leyvraz, P.F. (1999) "Strain rate effect on the mechanical behavior of the anterior cruciate ligament-bone complex", *Med. Eng. Phys.* **21**, 95–100, In Process Citation.
[24] Hayes, W.C. (1991) "Biomechanics of cortical and trbecular bone: implications for assesment of fracture risk", In: Hayes, W.C. and Mow, V.C., eds, Basic Orthopaedic Biomechanics (Raven Press, New York), pp. 93–142.
[25] Reilly, D.T., Burstein, A.H. and Frankel, V.H. (1974) "The elastic modulus for bone", *J. Biomech.* **7**, 271–275.
[26] Rice, J.C., Cowin, S.C. and Bowman, J.A. (1988) "On the dependence of the elasticity and strength of cancellous bone on apparent density", *J. Biomech.* **21**, 155–168.
[27] Kempson, G.E. (1979) "Mechanical properties of articular cartilage", In: Freeman, M.A.R., eds, Adult Articular Cartilage (Pitman Medical, Kent), pp. 333–414.